



Applicability of damage indices for detection of cracking in steel moment connections

B. Badrkhani Ajaei¹ and M. Ghassemieh^{2*}

1. M.Sc., School of Civil Engineering, University College of Engineering, University of Tehran, Tehran, Iran.

2. Associate Professor, School of Civil Engineering, University College of Engineering, University of Tehran, Tehran, Iran.

* Corresponding author: mghassem@ut.ac.ir

ARTICLE INFO

Article history:

Received: 22 September 2013

Accepted: 30 November 2013

Keywords:

Crack initiation

Moment resisting connections

Damage indices

Finite element method

Cyclic void growth model

ABSTRACT

Analytical detection of cracking in connections of steel moment resisting frames using simple damage indices is important since these cracks are not visible unless the connections are uncovered. In this paper, applicability of three cumulative damage indices for detection of cracking in a cover plate welded moment connection is investigated. The damage indices considered in this study are based on the following criteria: energy dissipation, plastic deformation and work index. Cracking of the connection is simulated for different loading histories by incorporating the cyclic void growth model to a finite element method of analysis of the connection. Results of simulation indicate good agreement with test results in terms of prediction of the cracking location and the instant of cracking. Based on the results of the performed simulations, the effects of the damage indices are compared. Overall, the energy dissipation damage index predicts cracking in this connection better than the other indices. Values of this index in the instant of cracking show little scatter for different loading histories.

1. Introduction

Observations after the Northridge earthquake signified that brittle fracture was the main cause of damage to the pre Northridge steel moment resisting connections [1]. These observations led to development of new connections with smaller initial flaws and high toughness weld and base metals, known as post Northridge connections. During the

subsequent tests on the post Northridge connections [2-5], it was observed that these connections were less prone to brittle fractures, and the main cause of damage to them was low cycle fatigue in the form of ductile crack initiation and growth. During an earthquake, cracks formed in connections of a building frame do not necessarily lead to fracture of connections; while, an aftershock or the next large earthquake may cause these

cracks to grow and lead to total fracture of the connections. In practice, some of the steel beam to column connections are set for visual inspection following an earthquake. However, detection of cracks using visual inspection requires removing the non-structural covering and therefore it can be very expensive when a large number of connections are to be inspected. Furthermore, small cracks may not be found by this method of inspection [2]. Consequently, considering the need to assess the safety of a structure after an earthquake, a computational method for detection of cracking in connections is needed.

Various indices for calculation of cumulative damage have been introduced in the literature, which are used to detect collapse of components, rather than cracking. The scope of this paper is to examine the ability of three cumulative damage indices in detecting cracking in a post Northridge cover plate connection.

A finite element model of the connection is developed in the ABAQUS finite element computer software [6]. Meanwhile, through a Fortran subroutine [7], a micromechanical model, i.e., Cyclic Void Growth Model (CVGM), is integrated into ABAQUS in order to simulate cracking in the connection. Based on the results of the CVGM, cumulative damage indices have been compared with each other.

2. Cumulative Damage Indices

The applicability of various cumulative damage indices for detection of cracking in moment connections are investigated in this paper. Three cumulative damage indices are selected based on their simplicity of use in assessment of structures [8]. These indices are described; as follows:

2.1. Energy Dissipation Index

The energy dissipation index is defined by the following relation:

$$D_{ce} = \sum_{i=1}^N \frac{E_i}{F_y \cdot S_y} \quad (1)$$

where E_i is the dissipated energy per cycle, F_y is the generalized yield force and S_y is the generalized yield displacement.

2.2. Cumulative Plastic Deformation Index

The cumulative plastic deformation index is based on accumulation of plastic deformations. It is defined by the following relation:

$$D_{ck} = \sum_{i=1}^N (\mu_{si} - 1)^a \quad (2)$$

in which

$$\mu_{si} = S_i / S_y \quad (3)$$

where S_i is the imposed displacement, and S_y is the yield displacement. Meanwhile, for equation 2, the value of a is set at 1.6, as suggested in [9].

2.3. Cumulative Work Index

The cumulative work index expresses the damage in terms of cumulative work, as defined by The following:

$$D_{ck} = \sum_{i=1}^N (\mu_{si} - 1) \lambda_i \quad (4)$$

in which,

$$\lambda_i = F_i / F_y \quad (5)$$

where F_i is the generalized force at the i^{th} cycle, F_y is the generalized yield force, and μ_{si} is the same as the one defined in equation 3.

3. Cyclic Void Growth Model

Structures subjected to earthquake loadings are normally excited with few number of load cycles (typically less than 20 cycles), with the strains that are well in excess of yield. The above phenomenon is in contrast to the conventional low cycle fatigue phenomenon, which involves cycles in the range of several hundreds to a thousand cycles, with much

smaller strains. Such conditions are termed as Ultra Low Cycle Fatigue (ULCF). Thus the mechanisms that cause ULCF are distinct from those that cause traditional low cycle fatigue [10].

The CVGM is introduced in [10] for simulation of ductile cracking (fracture initiation) in the ULCF regime. This model is based on the concept of growth and coalescence of voids in a metal matrix leading to formation of cracks [10,11].

In this model, cracking is predicted to occur, when

$$VGI_{cyclic} > VGI_{cyclic}^{critical} \quad (6)$$

where

$$VGI_{cyclic}^{critical} = VGI_{monotonic}^{critical} \exp(-\lambda \varepsilon_p^{accumulated}) \quad (7)$$

and

$$VGI_{cyclic} = \sum_{tensile\ cycles} \int_{\varepsilon_1}^{\varepsilon_2} \exp(1.5T) d\varepsilon_p - \sum_{compressive\ cycles} \int_{\varepsilon_1}^{\varepsilon_2} \exp(1.5T) d\varepsilon_p \quad (8)$$

in which, T is the stress triaxiality ratio, $d\varepsilon_p$ is the incremental plastic strain, ε_1 and ε_2 are the limits of integration corresponding to start and end of each cycle. $VGI_{monotonic}^{critical}$ and λ are material parameters calibrated by material tests, and $\varepsilon_p^{accumulated}$ is defined as the equivalent plastic strain that has accumulated up to the beginning of each tensile excursion of loading.

4. Cracking Simulation by CVGM

4.1. Investigated Connection

The RC03 connection subassembly tested in the Berkeley study [5], is used for the cracking simulations in this study. Fig. 1 shows the test setup and Fig. 2 shows the details of the connection. The connection considered was a cover plate connection consisted of a w30x99 (Gr.50) beam connected to a w14x176 (Gr.50) column. The beam flanges and rectangular

cover plates are joined to the column flange with groove welds; while, cover plates are attached to the beam flanges with both longitudinal and transverse fillet welds. The beam web and shear tab were groove welded to the column flange, while the shear tab was bolted to the beam web. Continuity plates were located on both sides of the column web, and a 10 mm doubler plate was used to strengthen the panel zone.

4.2. Finite Element Model

A three dimensional finite element model of the connection is developed by ABAQUS general purpose finite element software. The finite element model consists of 10468 quadratic hexahedral elements that utilize reduced integration (C3D20R) and 102 quadratic wedge elements (C3D15). The fillet welds are included in the model using

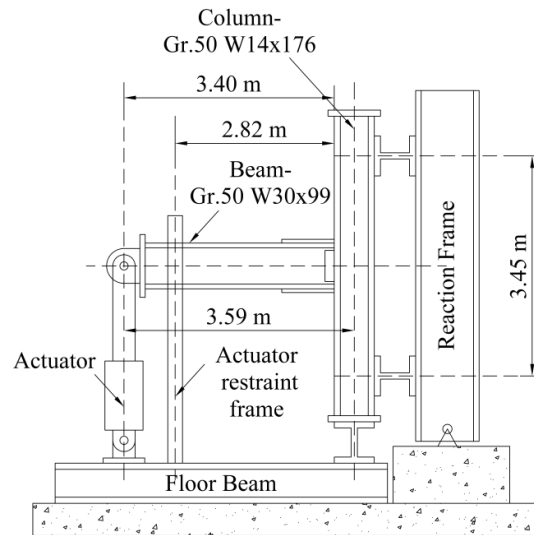


Fig. 1. Connection test setup

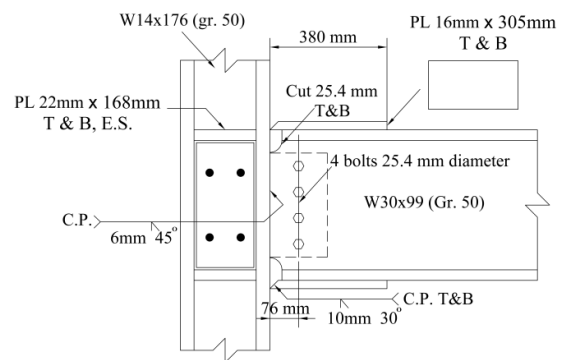


Fig. 2. Connection details

wedge elements, while groove welds are modeled by tie constraints between nodes.

For all materials, Young's modulus is set equal to 200,000 MPa, and Poisson's ratio is set equal to 0.3 [5]. Isotropic strain hardening is used in the material model. A tri-linear stress-strain relationship was used for all the material components with the properties presented in Table 1.

The finite element model is presented in Figs. 3 and 4. A geometric imperfection matching the first buckling mode shape of the model was introduced into the model.

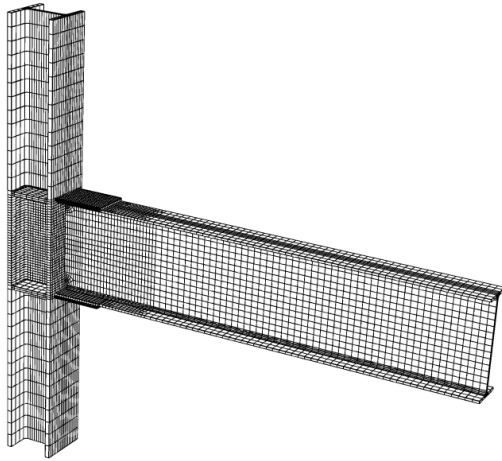


Fig. 3. Finite element mesh

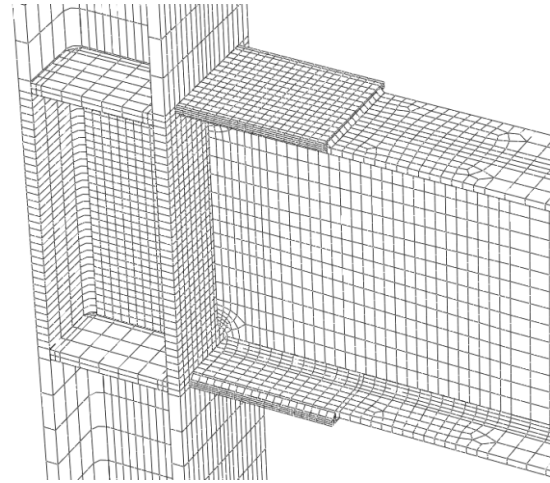


Fig. 4. Finite element mesh refinement in the region of connection

The maximum imperfection was chosen as 1 percent of the flange thickness. A Fortran subroutine developed by Myers et al. [7] is integrated into the finite element model in order to calculate CVGM variables at different integration points of the elements. $VGI_{monotonic}^{critical}$ and λ are set to be equal to 2.8 and 0.11 respectively. These values are obtained from coupon tests of a grade 50 steel material section [10].

Table 1. Mechanical properties of the connection components [5]

Component	Yield Stress (MPa)	Yield Strain	Ultimate Stress (MPa)	Ultimate Strain	Rupture Stress (MPa)	Rupture Strain
Beam Flange	369	0.0018	494	0.12	366	0.39
Beam Web	428	0.0022	506	0.12	435	0.39
Column Flange	350	0.0018	503	0.12	369	0.39
Column Web	386	0.0018	498	0.12	369	0.39
Reinforcing Plates	365	0.0018	497	0.12	366	0.39
Continuity Plates	365	0.0018	497	0.12	366	0.39
Fillet Welds	517	0.0026	552	0.12	517	0.39

4.3. Cracking Simulations

The connection was tested by the SAC basic loading protocol. The Loading histories applied to the finite element model are SAC basic and SAC near-fault loading histories [12] as illustrated in Fig. 5, and constant amplitude loading histories of 0.03, 0.04, and 0.05 radian

drift angles. Hereafter, results of the finite element analyses of the connection subjected to above loading histories are described briefly.

Fig. 6 compares the two load-drift diagrams of the RC03 connection subjected to the SAC basic loading history obtained by test [5] and

the finite element analysis. The diagrams are plotted up to the second 0.04 drift angle cycle; since cracking occurs during this cycle. Fig. 6 shows a satisfactory agreement between the test and finite element results.

Fig. 7 shows the contour of VGI_{cyclic} for the SAC basic loading protocol. In this figure, the point of maximum VGI_{cyclic} indicates the

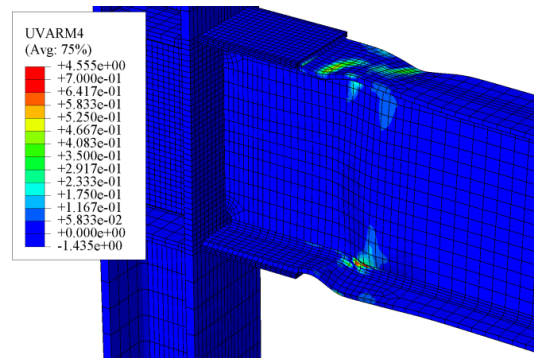


Fig. 7. Contour of VGI_{cyclic} for the SAC basic loading protocol

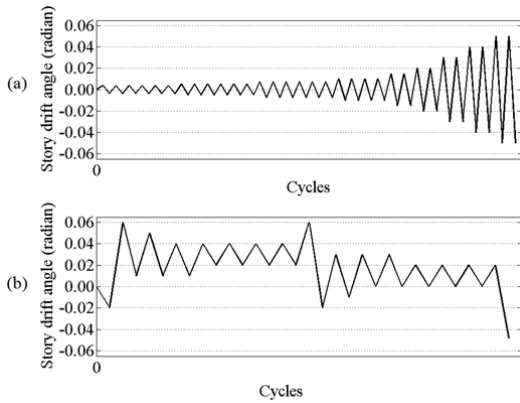


Fig. 5. SAC loading histories, (a) SAC basic loading history, (b) SAC near-fault loading history

location of cracking predicted by the CVGM. The prediction of cracking location shows good agreement with the location of initiation of fracture observed in the test [5]; (bottom flange of the beam, k-line region).

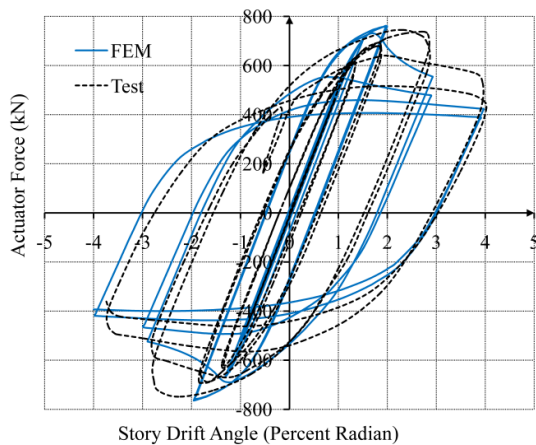


Fig. 6. load-drift diagrams of the connection for the SAC basic loading history

Fig. 8 illustrates the plots of VGI_{cyclic} and $VGI_{cyclic}^{critical}$ for the SAC basic loading protocol for the location of cracking. The instant of cracking is determined by intersection of these curves. This figure shows that cracking occurs during the second cycle of 0.04 drift angle, which is in agreement with the test result [5].

Cracking simulations for the other loading histories are performed using the same method. The VGI_{cyclic} and $VGI_{cyclic}^{critical}$ plots of other loading histories are presented in Figs. 9-12. The instant of cracking for all the loading protocols are presented in Table 2.

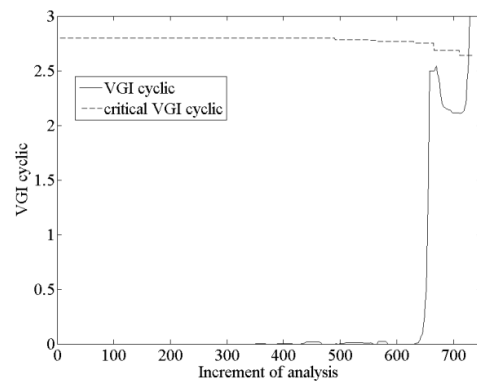


Fig. 8. VGI_{cyclic} and $VGI_{cyclic}^{critical}$ for the SAC basic loading history

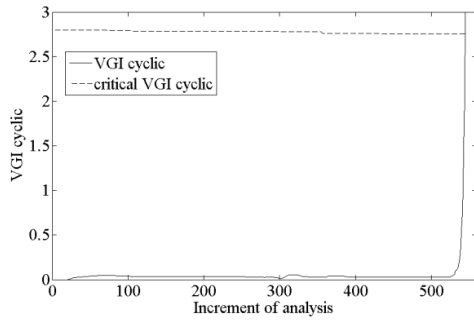


Fig. 9. VGI_{cyclic} and $VGI_{critical\ cyclic}$ for the SAC near-fault loading history

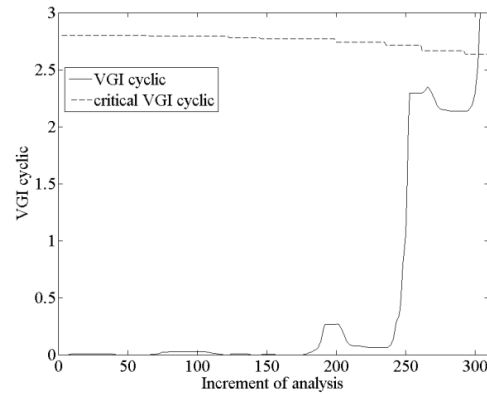


Fig. 12. VGI_{cyclic} and $VGI_{critical\ cyclic}$ for the constant amplitude (0.03 rad. drift) loading history

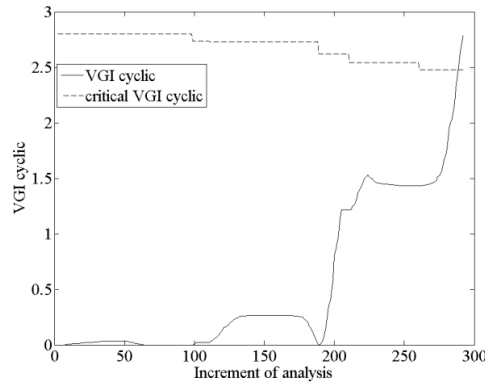


Fig. 10. VGI_{cyclic} and $VGI_{critical\ cyclic}$ for the constant amplitude (0.05 rad. drift) loading history

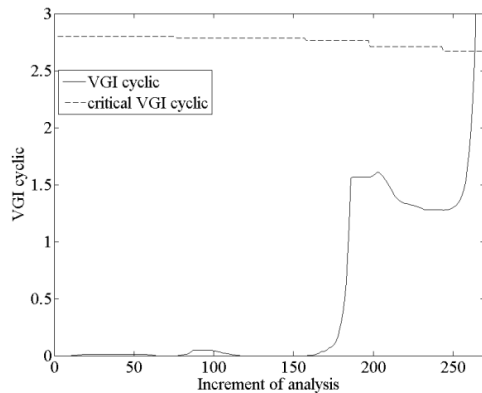


Fig. 11. VGI_{cyclic} and $VGI_{critical\ cyclic}$ for the constant amplitude (0.04 rad. drift) loading history

5. Comparison of Damage Indices

Based on the results of the CVGM simulation, the damage indices described in Section 2 are compared with each other. This is done in order to determine the index that results in better prediction of the instant of cracking in the connection considered.

The actuator force and displacement are chosen to be the generalized force and generalized displacement given in (1), (2) and (4). From the test results, the yield force is set equal to 747.6 kN and the yield displacement is set equal to 0.048 m [5]. In addition, the imposed displacements (S_i) are the displacements imposed on the beam tip in the

Table 2. Instant of cracking for the applied loading histories

Loading History	Instant of cracking
SAC basic	descending branch of second cycle of 0.04 drift
SAC near-fault	continuation of loading after ending of the loading history, drift angle of -0.048
Constant amplitude, 0.05 drift	descending branch of the third cycle
constant amplitude, 0.04 drift	descending branch of the third cycle
Constant amplitude, 0.03 drift	descending branch of the fifth cycle

finite element model, while the applied forces (F_i) are back calculated from the support reactions in the finite element model. Meanwhile, the sum of dissipated energy per cycles is calculated by evaluating the integral $\int F.ds$ numerically using the method of trapezoidal integration. The values of the damage indices calculated at the instant of cracking, for different loading histories, are presented in Table 3.

Considering the results presented in Table 3, it is evident that the energy dissipation index and the cumulative work index are more applicable for prediction of cracking in this connection, since each one of the two indices reach similar values for the various loading histories applied. This is confirmed by the coefficients of variation calculated for all those indices. The two indices mentioned above, are based on the assumption that certain amount of energy absorbed by the connection (i.e the work done by the external force) causes failure (cracking in this case) of the connection.

Table 3. Damage indices in the instant of cracking

Loading History	Energy dissipation index	Cumulative plastic deformation index	Cumulative work index
SAC basic	20.87	9.60	6.45
SAC Near-Fault	18.90	8.87	5.38
Constant amplitude, 0.05 drift	19.42	15.07	6.27
Constant amplitude, 0.04 drift	15.91	9.05	5.24
Constant amplitude, 0.03 drift	17.70	7.11	5.17
Mean	18.56	9.94	5.70
Coefficient of variation	0.10	0.30	0.11

Figs. 13 and 14 show the energy intake of the connection for the SAC basic and SAC near-fault loading histories, calculated by the numerical integration technique mentioned previously. In the figures presented, ascending branches of the curves represent the energy entered to the connection by external work, while the descending branches represent the energy which the connection gives back by returning elastic deformations at the beginning of each load reversal. Valleys of the curves give the amount of net dissipated energy after returning of elastic deformations in the beginnings of the load reversals.

As seen in Fig. 13 during cycles with amplitude less than the yield drift angle of 0.013, (i.e., before increment 300), the energy intake curve returns to zero at the beginning of each loading reversal. It is simply because the connection is in the elastic range during these cycles. However, as seen in Fig. 14, the cycles having amplitude of 0.01, corresponding to the increments 162-248 and 447-520, have non-zero contribution to energy dissipation, due to

occurrence of yielding and buckling in the previous large amplitude cycles.

The contribution of each cycle to the cumulative work index for SAC near-fault loading history is presented in Fig. 15. For cycles having amplitudes less than yield drift, the value of displacement ductility ratio, μ_{si} , becomes less than 1 resulting in negative values of $(\mu_{si} - 1)\lambda_i$ in (4) which are set equal to zero as shown in Fig. 15; since the meaning of the above expression in parenthesis is the ratio of inelastic deformations to the yield deformations. Consequently, this index is not capable of taking into account the effect of small cycles following large cycles.

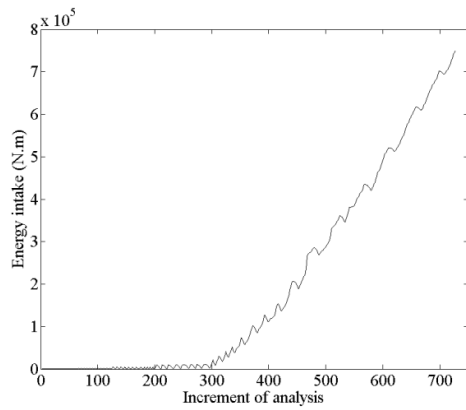


Fig. 13. Energy intake of the connection for SAC basic loading history

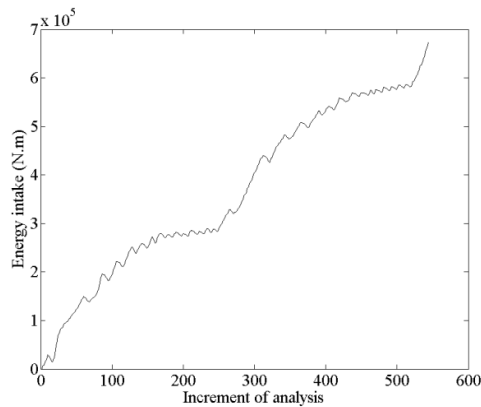


Fig. 14. Energy intake of the connection for SAC near-fault loading history

6. Conclusions

In this research, a finite element model of a cover plate welded moment connection is developed in the ABAQUS software environment. A FORTRAN subroutine is incorporated into the finite element model in order to simulate cracking in the connection utilizing cyclic void growth model. Comparison of the model simulation results with the test results showed good agreement in terms of prediction of the cracking location and the instant of cracking.

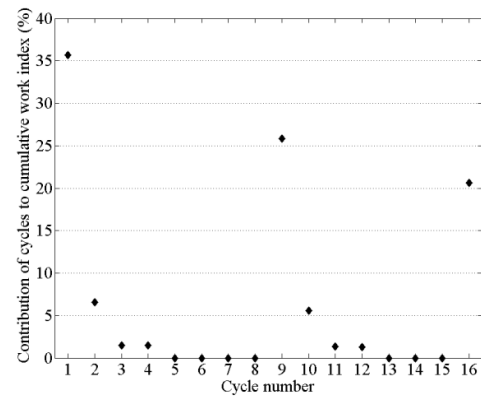


Fig. 15. Contribution of each cycle to the cumulative work index for SAC near-fault loading history

Applicability of three damage indices for detection of cracking in the connection is investigated. These damage indices are compared with each other, based on the results of cyclic void growth model simulations for five different loading histories. The results of the performed simulation studies indicated that the energy dissipation index results in better prediction of cracking in this connection. The cumulative plastic deformation index shows more scatter than the other indices. This shows the dependence of the index to loading history. The cumulative work index does not account for the effect of small amplitude cycles following large amplitude cycles. In addition, the method described in this paper can be used for calibrating a damage index for different types of connections.

Acknowledgement

The authors would like to thank Prof. Andrew T. Myers for giving permission for using the Fortran subroutine in this study.

REFERENCES

- [1] Kaufmann, E.J., Fisher, J.W., Di Julio Jr., R.M., Gross, J.L. (1997). "Failure analysis of welded steel moment frames damaged in the Northridge earthquake". NISTIR 5944, National Institute of Standards and Technology, Gaithersburg, Maryland.

- [2] Iyama, J., Ricles, J.M. (2009). "Prediction of fatigue life of welded beam-to-column connections under earthquake loading". *Journal of Structural Engineering (ASCE)*, Vol. 135, No. 12, pp. 1472-1480.
- [3] Zhang, X., Ricles, J.M., Lu, L.W., Fisher, J.W. (2004). "Analytical and experimental studies on seismic behavior of deep column-to-beam welded reduced beam section moment connections". *Proceedings of the 13th world Conference on Earthquake Engineering, Vancouver, Canada*, paper No. 1599.
- [4] Ricles, J.M., Zhang, X., Fisher, J.W., Lu, L.W. (2004). "Seismic performance of deep column-to-beam welded reduced beam section moment connections". *Proceedings of the 5th International Workshop on Connections in Steel Structures, Amsterdam*, pp. 211-222.
- [5] Kim, T., Whittaker, A.S., Gilani, A.S.J., Bertero, V.V., Takhirov, S.M. (2000). "Cover-plate and flange-plate reinforced steel moment-resisting connections". *Pacific Earthquake Engineering Research Center, Sacramento, California*.
- [6] ABAQUS, (1998). *User's Manual, Version 5.8*, Hibbitt, Karlsson, and Sorensen, Inc.
- [7] Myers, A.T., Deierlein, G.G., Kanvinde, A.M. (2009). "Testing and probabilistic simulation of ductile fracture initiation in structural steel components and weldments". Report No. 170, John A. Blume Earthquake Engineering Center, Stanford University, Palo Alto, CA.
- [8] Castiglioni, C.A., Pucinotti, R. (2009). "Failure criteria and cumulative damage models for steel components under cyclic loading". *Journal of Constructional Steel Research*, Vol. 65, No. 4, pp. 751-765.
- [9] Krawinkler, H., Zohrei, M. (1983). "Cumulative damage in steel structures subjected to earthquake ground motions". *Computers & Structures*, Vol. 16, No. 1-4, pp. 531-541.
- [10] Kanvinde, A.M., Deierlein, G.G. (2004). "Micromechanical simulation of earthquake induced fracture in steel structures". Report No. 145, John A. Blume Earthquake Engineering Center, Stanford University, Stanford, California.
- [11] Kanvinde, A.M., Deierlein, G.G. (2007). "Cyclic void growth model to assess ductile fracture initiation in structural steels due to ultra low cycle fatigue". *Journal of Engineering Mechanics (ASCE)*, Vol. 133, No. 6, pp. 701-712.
- [12] Krawinkler, H., Gupta, A., Medina, R., Luco, N. (2000). "Development of loading histories for testing of steel beam-to-column assemblies". Prepared for the SAC Steel Project, Department of Civil and Environmental Engineering, Stanford University, Palo Alto, California.